MAJOR ARTICLE

Postmortem Findings in Italian Patients With COVID-19: A Descriptive Full Autopsy Study of Cases With and Without Comorbidities

Laura Falasca,[1,a] Roberta Nardacci,[1,a] Daniele Colombo,[1] Eleonora Lalle,[1] Antonino Di Caro,[1] Emanuele Nicastri,[1] Andrea Antinori,[1] Nicola Petrosillo,[1] Luisa Marchioni,[1] Gianluigi Biava,[1] Gianpiero D'Offizi,[1] Fabrizio Palmieri,[1] Delia Goletti,[1] Alimuddin Zumla,[2,3,a] Giuseppe Ippolito,[1,a] Mauro Piacentini,[1,4,a] and Franca Del Nonno[1,a]; on behalf of COVID-19 INMI Study Group

[1]National Institute for Infectious Diseases Lazzaro Spallanzani-IRCCS, Rome, Italy, [2]Department of Infection, Division of Infection and Immunity, University College London, London, United Kingdom, [3]National Institute for Health Research Biomedical Research Centre, University College London Hospitals National Health Service Foundation Trust, London, United Kingdom, and [4]Laboratory of Cellular and Developmental Biology, Department of Biology, University of Rome Tor Vergata, Rome, Italy

Background. Descriptions of the pathological features of coronavirus disease-2019 (COVID-19) caused by the novel zoonotic pathogen severe acute respiratory syndrome coronavirus-2 (SARS-CoV-2) emanate from tissue biopsies, case reports, and small postmortem studies restricted to the lung and specific organs. Whole-body autopsy studies of COVID-19 patients have been sparse.

Methods. To further define the pathology caused by SARS-CoV-2 across all body organs, we performed autopsies on 22 patients with COVID-19 (18 with comorbidities and 4 without comorbidities) who died at the National Institute for Infectious Diseases Lazzaro Spallanzani-IRCCS Hospital, Rome, Italy. Tissues from the lung, heart, liver, kidney, spleen, and bone marrow (but not the brain) were examined. Only lung tissues were subject to transmission electron microscopy.

Results. COVID-19 caused multisystem pathology. Pulmonary and cardiovascular involvement were dominant pathological features. Extrapulmonary manifestations included hepatic, kidney, splenic, and bone marrow involvement, and microvascular injury and thrombosis were also detected. These findings were similar in patients with or without preexisting medical comorbidities.

Conclusions. SARS-CoV-2 infection causes multisystem disease and significant pathology in most organs in patients with and without comorbidities.

Keywords. autopsy; COVID-19; comorbidities; SARS-CoV-2; pathology.

The first human cases of coronavirus disease-2019 (COVID-19), caused by the novel zoonotic pathogen severe acute respiratory syndrome coronavirus-2 (SARS-CoV-2), were reported at the end of December 2019 in Wuhan, China. On 12 March 2020, the World Health Organization (WHO) declared COVID-19 a global pandemic as it rapidly spread worldwide [1]. In Italy, the first confirmed cases of COVID-19, reported on 31 January 2020, were 2 tourists from Wuhan, China. As of 19 August 2020, globally there have been 21 300 000 COVID-19 cases with 760 000 deaths reported to the WHO, of which Italy has reported 250 000 COVID-19 cases with 35 000 deaths [1].

Clinical and epidemiological studies have established that COVID-19 presents as a spectrum of clinical manifestations from asymptomatic, to mild illness (up to 80% of patients), moderate (15% of patients), to severe illness (5% of patients). Increased

mortality rates have been observed in older people (>70 years of age) and those with comorbidities [2, 3]. Reports from individual or small autopsy case studies [4–6] or limited postmortem studies [7–9] show that SARS-CoV-2, like SARS-CoV-1 in 2003, is a multisystem disease that predominantly affects the respiratory and cardiovascular system. SARS-CoV-2 has been detected in a range of clinical samples, such as bronchoalveolar lavage fluid, sputum, feces, and blood, indicating widespread dissemination [10]. Performing whole-body autopsies in patients who die of COVID-19 remains challenging due to infection control regulations and other logistical reasons [11, 12]. There is a need for more detailed and larger autopsy case series to further define the pathological manifestations of COVID-19 [13] and determine the full extent of organ involvement. Here, we reported the whole-body postmortem examinations of 22 Italian patients who died of COVID-19, 4 of whom had no comorbidities.

METHODS

Study Site and Ethical Approval

Autopsies were performed at the National Institute for Infectious Diseases Lazzaro Spallanzani-IRCCS Hospital, Rome, Italy. The study was approved by the local ethics committee (approval number 9/2020).

Study Cohort and Clinical Information

Patient demographic and clinical information was extracted from case records of 22 consecutive patients with COVID-19 who died and were autopsied.

Autopsy Procedures

Autopsies were performed using the specific guidance for post mortem, and collection according to submission of specimens and biosafety practices [11] to reduce the risk of transmission of infectious pathogens during and after postmortem examination. Because SARS-CoV-2 is classified as a biosafety level 3 (BSL3) organism, specific operating procedures for BSL3 pathogens were also followed. Autopsies were performed in a specific COVID-19 designated autopsy room with airflow control and airborne infection control procedures, including use of appropriated personal protective equipment (ie, National Institute for Occupational Safety and Health-certified disposable N-95 respirator).

SARS-CoV-2 RT-PCR

SARS-CoV-2 qualitative reverse transcriptase polymerase chain reaction (RT-PCR) testing for SARS-CoV-2 infection was performed on the following samples: ocular, nasopharyngeal, oropharyngeal, lung, and rectal swabs.

Tissues Sampled and Histological Stains

Tissues from the lung, heart, liver, kidney, spleen, and bone marrow were placed in formalin at room temperature for 72 hours before macroscopic analysis and processing for histological examination. The brain was not examined. Tissue samples were processed using hematoxylin and eosin staining (H&E), Masson trichrome stain, Perls stain, reticulin stain, periodic acid-Schiff reaction (PAS) and diastase-PAS. Giemsa and/or Grocott methenamine silver stains were performed where necessary.

Immunohistochemistry

Deparaffinized and rehydrated sections were used for immunohistochemistry. Organ sections were immersed in 10 mM sodium citrate, pH 6.0, and microwaved for antigen retrieval and stained on a BenchMark ULTRA system fully automated instrument (Roche) with an antibody directed against CD3 (2GV6; Ventana), CD4 (SP35; Ventana), CD8 (SP57; Ventana), CD15 (MMA; Ventana) CD26 (ab28340; Abcam), CD183 (1C6/CXCR3; BD Pharmigen), CD61 (ZfZ; Leica), CD20 (LZ6; Ventana), and CD68 (KP-1; Ventana).

Transmission Electron Microscopy

We only looked for evidence of SARS-CoV-2 in lung samples. Nonlung samples were not subject to transmission electron microscopy. Lung tissues were fixed with 2.5% glutaraldehyde in 0.1 M cacodylate buffer for 4 hours at 4°C. Fixation was performed with 1% OsO_4. Samples were then dehydrated in graded ethanol and embedded in Epon resin, as previously described [14, 15]. Ultrathin sections were stained with 2% uranyl acetate and examined under a transmission electron microscope (JEOL JEM 2100 Plus; Japan Electron Optics Laboratory). Images were captured with a digital camera (Tietz Video and Image Processing Systems).

RESULTS

Patient Demographics and Clinical Characteristics

Table 1 and Table 2 depict the demographic and clinical characteristics of 22 COVID-19 patients on whom postmortem examinations were performed. Of these, 18 had other medical comorbidities (designated group 1). Four patients were healthy prior to hospital admission and had no known medical comorbidities or any cause of immunosuppression (designated group 2).

Autopsy and Microscopic Examination
Lung Findings
Macroscopic Findings. Lungs from all patients were increased in volume, firm, edematous, and congested with diffuse pleural thickening and pleural effusion. Cut surface showed consolidation of lobes and red congested areas, with thickening of the interstitial septa and pulmonary edema (Figure 1A1). Subsegmental pulmonary embolism was seen in 5 cases.

Microscopic Findings. A range of common lung findings were seen on light microscopy. Parenchymal multifocal damage with intraalveolar exudative and proliferative inflammation (Figure 1A2), with fibrin, hyaline membranes (Figure 1A3) consistent with a diagnosis of diffuse alveolar damage (Table 3). Organizing pneumonia with fibrosis and type II pneumocyte hyperplasia, amphophilic cytoplasm, large nuclei, and prominent nucleoli, were indicative of cytopathic virus-induced changes

Table 1. Summary of Patient Demographics at Baseline

| Characteristic	Group 1 With Comorbidities	Group 2 Without Comorbidities
Number of patients	18	4
Demography		
Age, y, median ± SD (range)	76 ± 15.7 (27–92)	48.5 ± 13.07 (35–65)
Men	12 (66.7)	3 (75)
Women	6 (33.3)	1 (25)
Comorbidity		
Chronic obstructive pulmonary disease	6 (33.3)	…
Cardiac disease	8 (44.5)	…
Malignancy	5 (27.8)	…
Hypertension	4 (22.3)	…
Diabetes	4 (22.3)	…
Schizophrenia	1 (5.6)	…
Kidney disease	2 (11.2)	…

Data are No. (%) except where indicated.

Table 2. Demographics, Comorbidities, Duration of Hospital Stay, and Autopsy Cause of Death

Patient Number	Sex, M/F	Age, y	Onset of Symptoms, d	Comorbidities	Days in Hospital Before Death	Postmortem Cause of Death
1	M	81	Not known	Hypertension Aortomyocardial sclerosis Ischemic heart disease Cardiomyopathy Aortic aneurysm	4	Cardiorespiratory failure
2	F	82	Not known	Diabetes Atrioventricular valve prothesis Atrial fibrillation COPD Malignancy Kidney disease	3	Cardiorespiratory failure
3	M	92	7	COPD	1	Cardiorespiratory failure
4	F	69	Not known	Schizophrenia	28	Cardiorespiratory failure
5	F	80	Not known	Cardiovascular disease Senile dementia	38	Cardiorespiratory failure
6	M	92	Not known	Cardiovascular disease COPD	3	Cardiorespiratory failure
7	F	64	4	Malignancy	2	Cardiorespiratory failure
8	M	58	Not known	Pulmonary artery thrombosis	4	Cardiorespiratory failure
9	M	64	Not known	Myelodysplasia	4	Cardiorespiratory failure
10	M	82	3	Aortic aneurysm COPD	5	Cardiorespiratory failure
11	M	76	Not known	Malignancy	30	Cardiorespiratory failure
12	M	60	6	Malignancy Hypertension Kidney disease Diabetes COPD Obesity	29	Cardiorespiratory failure
13	F	70	Not known	Cardiovascular disease Diabetes Psychiatric disorder	43	Cardiorespiratory failure
14	M	76	Not known	Malignancy COPD Hypertension Cardiovascular disease	33	Cardiorespiratory failure
15	F	27	Not known	HIV infection	6	Cardiorespiratory failure
16	M	82	Not known	Parkinson disease Hypertension Transient ischemic attack Prostate hypertrophy	14	Cardiorespiratory failure
17	M	57	Not known	Diabetes	1	Cardiorespiratory failure
18	M	86	Not known	Endocarditis caused by *Staphylococcus aureus* Prostate hypertrophy Aortic aneurysm Atrial fibrillation	1	Cardiorespiratory failure
19	M	54	4	NONE	16	Cardiorespiratory failure
20	M	35	5	NONE	7	Cardiorespiratory failure
21	M	65	7	NONE	12	Cardiorespiratory failure
22	F	43	Not known	NONE	25	Cardiorespiratory failure

Abbreviation: COPD, chronic obstructive pulmonary disease.

(Figure 1A3 and 1A4). Fibroblastic foci consisting of loose organizing connective tissue reflective of alveolar duct fibrosis were seen (fibrotic phase) (Figure 1B1). Other findings included: pleural fibrosis (Figure 1B4), vascular injury with thrombi (Figure 1B2), and vasculitis (Figure 1B3). A main feature was the presence of numerous inflammatory cells consisting of granulocytes (CD15^{+}) (Supplementary Figure 1A1 and 1A2), macrophages (CD68^{+})

(Supplementary Figure 1A3 and 1A4), and T lymphocytes (CD3^{+}) infiltrating into alveolar septa and clustering around capillary vessels (Supplementary 1B1). Immunohistochemistry showed the presence of both CD4^{+} and CD8^{+} T lymphocytes (Supplementary Figure 1B2 and 1B3). Of note, lymphocytes were CD20^{−} indicating an absence of infiltrating B lymphocytes. Thrombi were present and immunohistochemistry showed
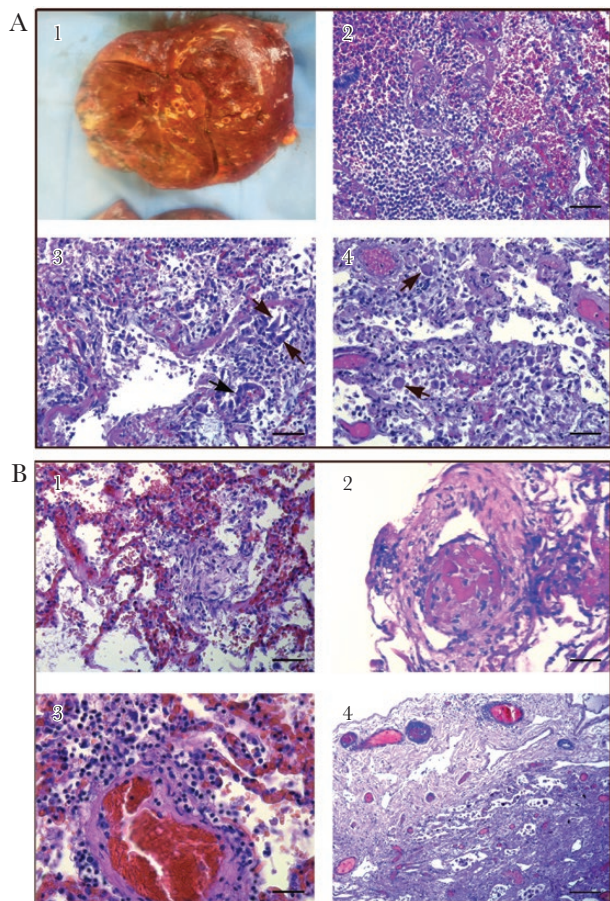
Figure 1. Pathological findings in lung. *A1*, Lungs showed an increase in volume and were firmer and heavier than normal. *A2* and *A3*, Light microscopic analysis shows parenchymal multifocal damage with intraalveolar inflammation, fibrin, and hyaline membranes consistent with a diagnosis of diffuse alveolar damage. Both acute exudative inflammatory process and fibrous proliferative phase were found. *A3* and *A4*, Hyperplasia of type II pneumocyte, characterized by amphophilic cytoplasm, large nuclei, and prominent nucleoli, are shown (arrows). *B1*, Alveolar duct fibrosis. *B2*, Fibrin thrombi in capillaries. *B3*, Vascular injury including vessel vasculitis and vascular edema. *B4*, Pleural fibrosis. Abbreviation: H&E, haematoxylin and eosin. Scale bars: *A2*, 14 µm; *A3–B3*, 7 µm; *B4*, 21 µm.

the presence of platelet aggregates and megakaryocytes within thrombi (Supplementary Figure 1B4).

Immunohistochemistry Findings. T-cell activation is modulated by dipeptidyl peptidase-4 (DPP4) [16] and thus the expression of CD26/DPP4 and CXCR3/CD183 was analyzed on lung tissues from group 2 patients (Figure 2). Numerous CD26⁺ cells were found in the alveolar septa (Figure 2A1–2A3) with intense staining seen in the type II pneumocytes (Figure 2A3). Positive cells entrapped with fibrin clots in the vascular lumen were also observed (Figure 2A4). CXCR3 immunostaining showed lymphocytes localized in inflammatory perivascular aggregates (Figure 2B1, 2B2, and 2B4) which spread into alveolar septa and alveolar spaces (Figure 2B2 and 2B3).

Table 3. Histopathology Findings

Findings	Group 1, No. (%) (n = 18)	Group 2, No. (%) (n = 4)
Lung		
Hyaline membranes	8 (44.4)	2 (50.0)
Hyperplasia of type II pneumocyte	11 (61.2)	4 (100)
Alveolar plug	8 (44.4)	4 (100)
Alveolar fibrin deposit	9 (50.0)	3 (75.0)
Hemorrhage	10 (55.6)	2 (50.0)
Inflammatory cells	13 (72.3)	4 (100)
Diffuse alveolar damage, fibrotic phase	12 (66.7)	1 (25.0)
Microthrombi	14 (77.8)	2 (50.0)
Vasculitis	8 (44.4)	4 (100)
Multinucleated giant cells	4 (22.3)	2 (50.0)
Cardiac		
Myocarditis	9 (50.0)	3 (75.0)
Vasculitis	5 (27.8)	3 (75.0)
Inflammatory infiltrate	13 (72.3)	3 (75.0)
Focal necrosis	6 (33.4)	2 (50.0)
Pericarditis	9 (50.0)	4 (100)
Vascular fibrosis	4 (22.3)	2 (50.0)
Hepatic		
Inflammatory infiltrate	8 (44.4)	3 (75.0)
Congestion	8 (44.4)	2 (50.0)
Steatosis	9 (50.0)	3 (75.0)
Renal		
Inflammatory infiltrate	9 (50.0)	3 (75.0)
Glomerulosclerosis	9 (50.0)	3 (75.0)
Interstitial fibrosis	9 (50.0)	4 (100)
Splenic		
Congested red pulp	15 (83.4)	4 (100)
Lymphoid hypoplasia	11 (61.2)	4 (100)
Bone marrow		
Megakaryocytes hyperplasia	0	2 (50.0)
Adipocytes	7 (38.9)	1 (25.0)

Electron Microscopic Findings. SARS-CoV-2 particles were detected within type II pneumocytes, which showed degenerating features characterized by fine and uniformly dispersed chromatin. These pneumocytes displayed swollen mitochondrial profiles and dilated rough endoplasmic reticulum (Figure 3). Numerous virus-containing compartments (VCC) of different sizes and shapes were detected (Figure 3A, 3B, and 3D). Interestingly, spherules, very small vesicles containing single viral particles (Figure 3B and 3C), were also observed.

Heart Findings
Macroscopic Findings. The hearts in all group 1 and **2** patients showed increased size and weight, hypertrophy, and dilation of the left and right atria and ventricles. The myocardium appeared pale and flabby, and endocardium showed punctuate petechial hemorrhages (Figure 4A1). Some patients in group 1 had pathological changes that were related to the patient's age. These included myocardial ischemic or inflammatory changes,
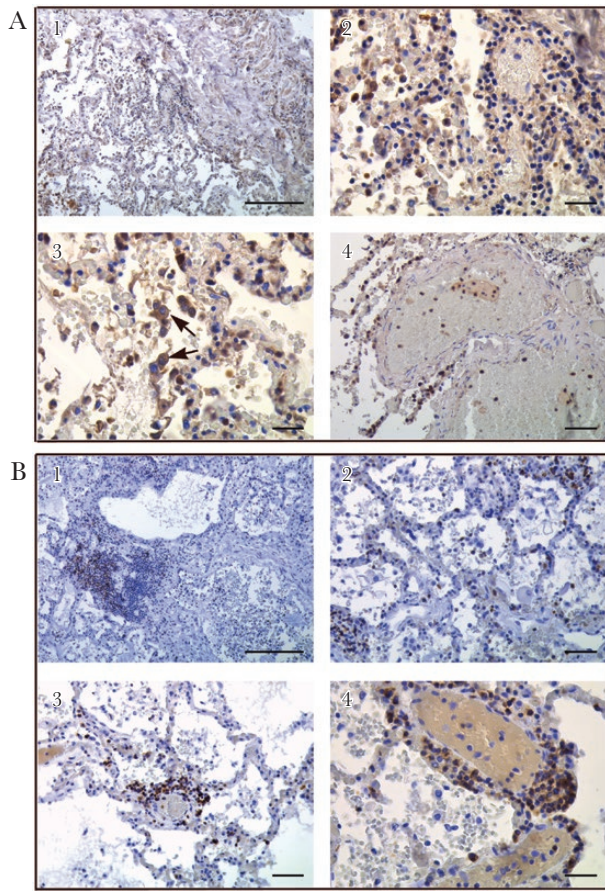
Figure 2. Immunohistological characterization of lung tissue. *A1–A4*, CD26/dipeptidyl peptidase-4 expression in lung tissue. Numerous strongly positive CD26$^+$ cells are seen in the alveolar septa. *A3*, Intense staining is seen in the type II pneumocytes (arrows). *A4*, Positive cells are also seen entrapped with fibrin in the vascular lumen. *B1–B4*, CXCR3/CD183 immunostaining shows intense staining of lymphocytes localized in the inflammatory perivascular aggregates and spread into alveolar septa and alveolar spaces. Scale bars: *A1* and *B1*, 100 μm; *A2, A3*, and *B4*, 7 μm; *A4, B2*, and *B3*, 14 μm.

hypertensive changes of the left ventricular cavity, and valvular calcification of the mitral annulus and aortic valve (Figure 4A2).

Microscopic Findings. Microscopic changes seen were hypertrophy of myocytes and variable degrees of interstitial and vascular fibrosis (Figure 4A3 and 4A4). Mononuclear cells infiltrating adventitia was found predominantly in group 2 patients (Figure 4A4). Active myocarditis (Figure 4B1) characterized by mononuclear, predominantly lymphocytic, infiltrate, and was associated with focal myocytes necrosis (Figure 4B2), fibrinous, and hemorrhagic areas with myofibers disarray (Figure 4B3). Pericarditis (fibrinous or fibrous) was seen mainly in group 2 patients (Figure 4B4).

### Liver, Kidney, Spleen, and Bone Marrow Findings

Liver. Macroscopic inspection of the liver of all patients showed parenchyma congestion. The main findings at histological level were sinusoidal congestion and extravasation of red blood cells into the space of Disse (Figure 5A1) and in a few cases this was associated with congestion of small veins and hepatocyte necrosis (Figure 5A2 and 5A3) and infiltration (Figure 5A4). Macrovacuolar and microvacuolar steatosis was seen mostly in group 2 patients (Figure 5A1, 5A2, and 5A4, and Table 3).

Kidney. The kidneys of all patients generally had normal shape with reduced volume and size. Outer surfaces showed reddish depressions. Histological examination showed interstitial fibrosis, mainly in group 2 patients (Figure 5B1), with swollen glomerular endothelial cells. Fibrin deposits were visible underneath the Bowman capsule (Figure 5B2). Chronic tubular-interstitial inflammation (Figure 5B3) and glomerular sclerosis were observed (Figure 5B4) even in patients without a history of previous kidney disease (Table 3).

Spleen. The spleens of all patients had normal shape but reduced volume and size. The splenic white pulps of all 4 of the group 2 cases showed lymphoid hypoplasia with congested red pulp (Figure 6A1 and 6A2), and Table 3).

Bone Marrow. Microscopic analysis of the bone marrows generally showed replacement of red hematopoietic bone marrow with yellow adipocyte-rich marrow in group 1 patients (Figure 6B1). Megakaryocytes hyperplasia (Figure 6B2) was seen in 2 patients of group 2 (Table 3). Numerous macrophages (CD68$^+$) were seen and they displayed features of hemophagocytosis (Figure 6C1 and 6C2).
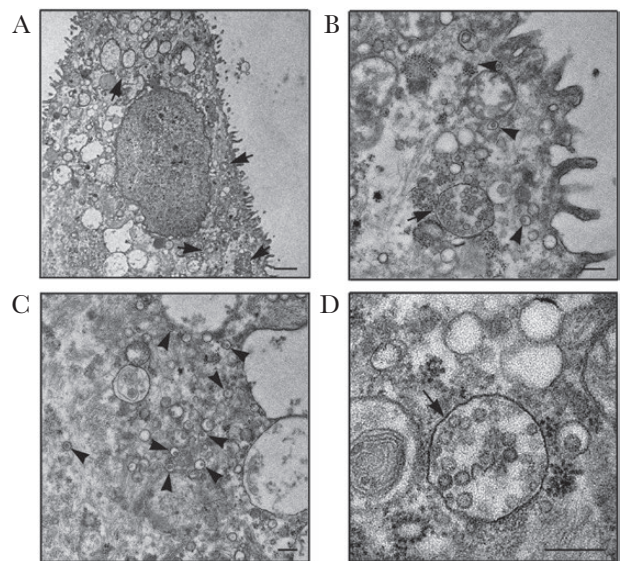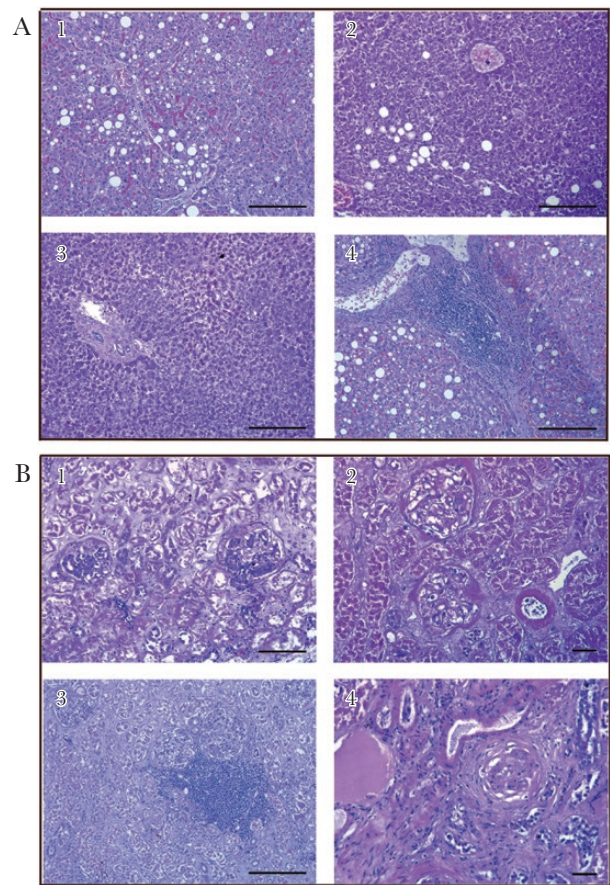

Figure 3. SARS-CoV-2 detection in lung tissue by transmission electron microscopy. *A*, SARS-CoV-2 particles are visible in virus-containing compartments in type II pneumocytes (arrows). *B–D*, Numerous viral particles are enclosed in single-membrane vacuoles (arrow). Other, very small vesicles contain single viral particles (arrowheads). Scale bars: *A*, 1 μm; *B–D*, 200nm.
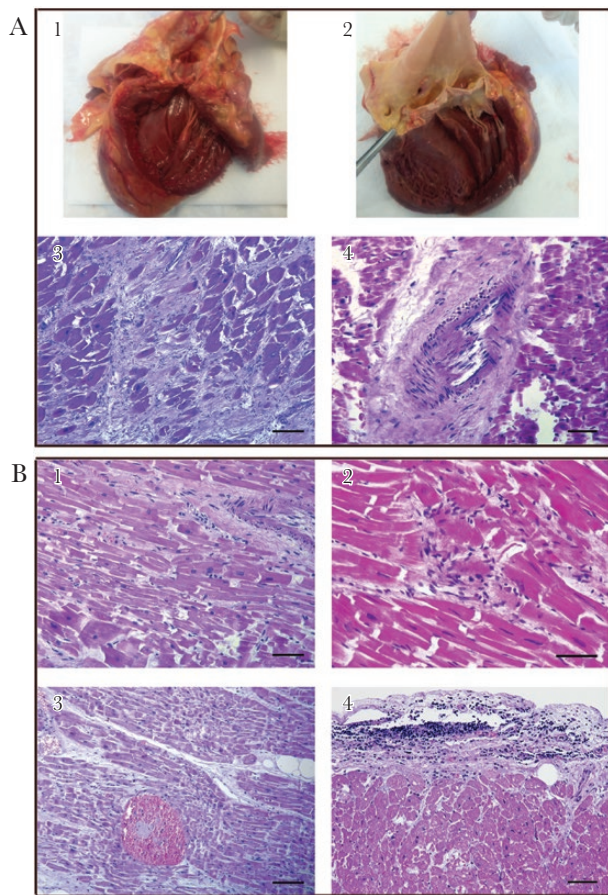
Figure 4. Histological changes in heart. *A1*, Hearts were increased in size and weight. The myocardium appeared pale and flabby. Endocardium showed punctuate petechial hemorrhages. *A2*, Age-related disease of the heart was represented by volume changes of the left ventricular cavity and exacerbated by systemic hypertension with valve changes including calcification of the mitral annulus and aortic valve. *A3* and *A4*, Heart tissue shows myocytes hypertrophy, and variable degrees of interstitial and vascular fibrosis with mononuclear cells infiltrating adventitia. *B1*, Active myocarditis was characterized by mononuclear, predominantly lymphocytic infiltrate, associated with focal myocytes necrosis (*B2*). *B3*, Fibrinous, hemorrhagic areas with myofibers disarray were present. *B4*, Pericarditis with lymphocytic infiltration and increase in fibrous tissue was seen in all patients. Abbreviation: H&E, haematoxylin and eosin. Scale bars: *A3* and *B4*, 21 µm; *A4–B2*,7 µm; *B3*, 14 µm.

Figure 5. Pathological findings in liver and kidney. *A1*, Liver tissue shows sinusoidal congestion and extravasation of red blood cells into the space of Disse. In some cases, small vein congestion (*A2*) and hepatic necrosis (*A3*) were reported. *A4*, Inflammatory infiltration was observed. *A1*, *A2*, and *A4*, Macrovacuolar and microvacuolar steatosis were observed in the majority of cases. *B1*, Kidney glomerular endothelial cells were swollen. *B2*, Fibrin deposit is visible underneath the Bowman capsule. *B3*, Tubulointerstitial inflammation and (*B4*) glomerular sclerosis were observed. Abbreviation: H&E, haematoxylin and eosin. Scale bars: *A1–A4*, and *B3*, 50 µm; *B1*, *B2*, and *B4*, 14 µm

DISCUSSION

Whole-body autopsies offer several advantages over limited sampling using biopsies and tissues obtained post mortem [4–7]. Full-body autopsy studies of COVID-19 patients have been few due to several issues of infection control, and logistical and operational reasons. Whole-body autopsy allows examination of most body organs to define the extent of COVID-19 pathology, and also allows adequate tissue to be obtained for further pathological and molecular evaluation and for research purposes. They also allow a more accurate diagnosis to be made and minimize the chances of missing an accurate diagnosis due to sampling error. Supporting the call for action to conduct full autopsies on patients who die of COVID-19 for determining the extent of organ involvement [12, 13], we conducted a comprehensive postmortem full autopsy examination of 22 patients. To our knowledge, our study is the first to report pathological features of 4 cases of COVID-19 who did not have any prior underlying comorbidity or causes of immunosuppression.

Our observations add further information on the pathology examination findings of COVID-19. An initial report from China described histopathological findings in 2 cancer patients with COVID-19, which showed several nonspecific histological changes, edema, fibrinous, proteinaceous exudates, hyperplastic pneumocytes, patchy inflammation, and multinucleated giant cells [4]. A case report, also from China, described findings in a postmortem biopsy specimen which showed diffuse alveolar damage and interstitial mononuclear inflammatory infiltrates [5]. In our autopsy study, we found that COVID-19 predominantly causes acute lung injury and diffuse alveolar damage,
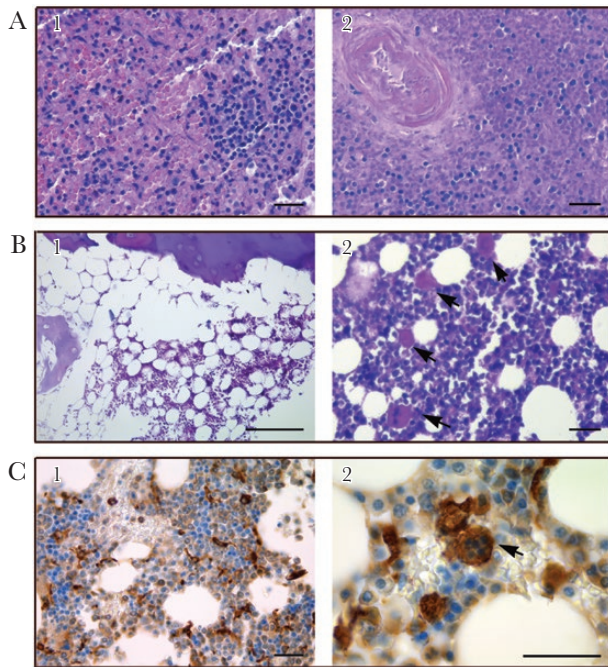
Figure 6. Histology of spleen and bone marrow. *A1* and *A2*, Lymphoid hypoplasia is visible in the splenic white pulp. *B1* and *B2*, Bone marrows tissue shows replacement of red hematopoietic bone marrow with yellow adipocyte-rich marrow. Megakaryocyte hyperplasia is observed (arrows). Abbreviation: H&E, haematoxylin and eosin. *C1*, Macrophages (CD68^{+}) are present in bone marrow tissue. *C2*, CD68^{+} cells displaying features of hemophagocytosis (arrow). Scale bars: *A1, A2, B2–C2*, 7 μm; *B1*, 100 μm.

which is associated with multisystem involvement and significant pathology across most body organs in patients with and without comorbid disease. All deaths were due to cardiorespiratory failure and all cases had extrapulmonary manifestations. Microvascular injury and thrombosis were also detected. The 4 younger patients without preexisting medical conditions also had similar findings despite absence of comorbidities and displayed all the histopathological hallmarks of widespread vascular injury, including liver, kidney, spleen, and bone marrow involvement.

Our lung pathology findings were similar to those seen in a study of postmortem lung tissues from northern Italy of 33 males and 5 female patients, with an average age of 69 years (range 32–86) [17]. In addition, using electron microscopy we identified viral particles in the cytoplasm of type II pneumocytes—the main target of viral infection [18]. Interestingly, all the histological hallmarks of interstitial pneumonia and capillary damage were prominent in all 22 COVID-19 cases, with T lymphocytes being prominent in vascular infiltrates (vasculitis) and interstitial inflammation.

Clinical studies have indicated that acute respiratory distress syndrome and multiple organ failure are features of severe cases of COVID-19. These are thought to be underpinned by an excessive immune response [19]. In the lung microenvironment,

excessive inflammatory cytokine may be caused by immune-pathological changes linked to lymphocytic infiltration. We demonstrated a significant upregulation of the chemokine receptor CXCR3, which is not only responsible for T cells extravasating from blood vessels and migration [20], but it has been also implicated in pulmonary fibrosis [21]. It is thus possible that this is associated with an aberrant type I immune response involving the CXCR3/ligand pathway. In addition, we found intense expression of CD26/DPP4, a protein that plays a key role in T-cell signal transduction processes as a costimulatory molecule, and its expression level is known to correlate with the severity of inflammation [22]. Thus, the CXCR3 cytokine axis could be considered a potential therapeutic target in development of targeted host-directed therapies for COVID-19.

Several publications have shown an association of the severity of the clinical expression of COVID-19 with the number of comorbidities present. Cardiac involvement in severe COVID-19 pathogenesis has been well documented [23], and cardiac risk factors have been identified as risk factors for increased mortality [24]. In our study of the macroscopic and microscopic features of hearts we found several differences between patients with and without comorbidities. The 4 cases without comorbidities showed pronounced pericarditis and inflammatory cells infiltrating adventitia, indicating that the heart can be compromised irrespective of previous cardiovascular disease. Kidney injury has been reported in nearly 30% of COVID-19 patients [25]. We found that histopathological changes in kidney in patients without comorbidities appeared more severe that those with comorbidities. Patients without comorbidities also showed greater hepatic injury. Whether these findings represent liver or kidney damage caused directly by SARS-CoV-2 itself or are a reflection of the consequences of an abnormal and excessive inflammatory response, requires definition [26]. Studies of other viral infections of the respiratory tract have shown that liver injury may be immune mediated or a result of direct cytopathic damage [27].

Our study showed that the spleen and bone marrow were affected in 2 of 4 of our patients without comorbidities. Microscopic analyses of bone marrow showed white pulp lymphoid hypoplasia and megakaryocyte hyperplasia. These hematopoietic organs could be reservoirs of SARS-CoV-2 infection [28] and may directly infect hematopoietic stem/progenitor cells, megakaryocytes, and platelets [29]. Microvascular damage and thrombosis were also a prominent feature in cases with and without comorbidities. This supports the observation that anticoagulant treatment can reduce mortality in COVID-19 [30]. Patients with COVID-19 who do not have comorbidities appear to have similar pathological manifestations as those with comorbidities [31].

There were some limitations of our study. Whilst the COVID-19 cases in our study were from a range of age, sex, and comorbidities, we cannot accurately say our findings are fully

representative of COVID-19 pathology in the large numbers who have died in Italy. A range of neurological manifestations of COVID-19 have been reported [32]; however, we were unable to obtain brain tissue in our study. A recent [33] histopathological examination of brain specimens obtained from COVID-19 patients who died up to 32 days after symptom onset found only hypoxic changes and no specific brain changes attributable to SARS-CoV-2. Further pathological examination of brain tissues needs to be performed where cytoplasmic viral staining, immunohistochemical, and electron microscope analysis may shed further light on the neuropathological manifestations of COVID-19. It is important that autopsy studies are given priority. Whole-body complete autopsy studies from across a wide range of geographical background, age, ethnic group, and comorbidities [10, 34, 35] are required to define the pathogenesis and the complete spectrum of pathology in COVID-19.

Supplementary Data

Supplementary materials are available at *The Journal of Infectious Diseases* online. Consisting of data provided by the authors to benefit the reader, the posted materials are not copyedited and are the sole responsibility of the authors, so questions or comments should be addressed to the corresponding author.

Notes

References

1. World Health Organization. Coronavirus disease (COVID-19) situation reports. https://www.who.int/emergencies/diseases/novel-coronavirus-2019/situation-reports. Accessed 14 July 2020.
2. Chen N, Zhou M, Dong X, et al. Epidemiological and clinical characteristics of 99 cases of 2019 novel coronavirus pneumonia in Wuhan, China: a descriptive study. Lancet **2020**; 395:507–13.
3. Chen G, Wu D, Guo W, et al. Clinical and immunological features of severe and moderate coronavirus disease-2019. J Clin Invest **2020**; 130:2620–9.
4. Xu Z, Shi L, Wang Y, et al. Pathological findings of COVID-19 associated with acute respiratory distress syndrome. Lancet Respir Med **2020**; 8:420–2.
5. Tian S, Xiong Y, Liu H, et al. Pathological study of the 2019 novel coronavirus disease (COVID-19) through post-mortem core biopsies. Mod Pathol **2020**; 33:1007–14.
6. Konopka KE, Wilson A, Myers JL. Postmortem lung findings in a patient with asthma and coronavirus disease 2019. Chest **2020**; 158:e99–101.
7. Su H, Yang M, Wan C, et al. Renal histopathological analysis of 26 postmortem findings of patients with COVID-19 in China. Kidney Int **2020**; 98:219–27.
8. Wichmann D, Sperhake JP, Lütgehetmann M, et al. Autopsy findings and venous thromboembolism in patients with COVID-19: a prospective cohort study. Ann Intern Med **2020**; 173:268–77.
9. Menter T, Haslbauer JD, Nienhold R, et al. Postmortem examination of COVID-19 patients reveals diffuse alveolar damage with severe capillary congestion and variegated findings of lungs and other organs suggesting vascular dysfunction [published online ahead of print 4 May 2020]. Histopathology doi: 10.1111/his.14134.
10. Yuan Y, Wang N, Ou X. Caution should be exercised for the detection of SARS-CoV-2, especially in the elderly [published online ahead of print 30 March 2020]. J Med Virol doi: 10.1002/jmv.25796.
11. Hanley B, Lucas SB, Youd E, Swift B, Osborn M. Autopsy in suspected COVID-19 cases. J Clin Pathol **2020**; 73:239–42.
12. Ledford H. Autopsy slowdown hinders quest to determine how coronavirus kills. [published online ahead of print 7 May 2020]. Nature doi: 10.1038/d41586-020-01355-z.
13. Barth RF, Xu X, Buja LM. A call to action: the need for autopsies to determine the full extent of organ involvement associated with COVID-19. Chest **2020**; 158:43–4.

14. Baiocchini A, Del Nonno F, Taibi C, et al. Liver sinusoidal endothelial cells (LSECs) modifications in patients with chronic hepatitis C. Sci Rep **2019**; 9:8760. Erratum in: Sci Rep 2020; 10:1420.

15. Nardacci R, Amendola A, Ciccosanti F, et al. Autophagy plays an important role in the containment of HIV-1 in nonprogressor-infected patients. Autophagy **2014**; 10:1167–78.

16. Klemann C, Wagner L, Stephan M, von Hörsten S. Cut to the chase: a review of CD26/dipeptidyl peptidase-4's (DPP4) entanglement in the immune system. Clin Exp Immunol **2016**; 185:1–21.

17. Carsana L, Sonzogni A, Nasr A, et al. Pulmonary post-mortem findings in a series of COVID-19 cases from northern Italy: a two-centre descriptive study [published online ahead of print 8 June 2020]. Lancet Infect Dis doi: 10.1016/S1473-3099(20)30434-5.

18. Nardacci R, Colavita F, Castilletti C, et al. SARS-CoV-2 cytopathogenesis in cultured cells and in COVID-19 autoptic lung, evidences of lipid involvement. Research Square [Preprint] **7** July **2020** [cited 9 September 2020]. Available from https://doi.org/10.21203/rs.3.rs-39274/v1.

19. Ye Q, Wang B, Mao J. The pathogenesis and treatment of the 'cytokine storm' in COVID-19. J Infect **2020**; 80:607–13.

20. Moser B, Wolf M, Walz A, Loetscher P. Chemokines: multiple levels of leukocyte migration control. Trends Immunol **2004**; 25:75–84.

21. Jiang D, Liang J, Hodge J, et al. Regulation of pulmonary fibrosis by chemokine receptor CXCR3. J Clin Invest **2004**; 114:291–9.

22. Kruschinski C, Skripuletz T, Bedoui S, et al. CD26 (dipeptidyl-peptidase IV)-dependent recruitment of T cells in a rat asthma model. Clin Exp Immunol **2005**; 139:17–24.

23. Zhang H, Penninger JM, Li Y, Zhong N, Slutsky AS. Angiotensin-converting enzyme 2 (ACE2) as a SARS-CoV-2 receptor: molecular mechanisms and potential therapeutic target. Intensive Care Med **2020**; 46:586–90.

24. Aghagoli G, Gallo Marin B, Soliman LB, Sellke FW. Cardiac involvement in COVID-19 patients: risk factors, predictors, and complications: a review. J Card Surg **2020**; 35:1302–5.

25. Diao B, Feng Z, Wang C, et al. Human kidney is a target for novel severe acute respiratory syndrome coronavirus 2 (SARS-CoV-2) infection. medRxiv [Preprint]. **10** April **2020** [cited 9 September 2020]. Available from: https://doi.org/10.1101/2020.03.04.20031120.

26. Xu L, Liu J, Lu M, Yang D, Zheng X. Liver injury during highly pathogenic human coronavirus infections. Liver Int **2020**; 40:998–1004.

27. Feng G, Zheng KI, Yan QQ, et al. COVID-19 and liver dysfunction: current insights and emergent therapeutic strategies. J Clin Transl Hepatol **2020**; 8:18–24.

28. Gu J, Gong E, Zhang B, et al. Multiple organ infection and the pathogenesis of SARS. J Exp Med **2005**; 202:415–24.

29. Yang M, Ng MH, Li CK. Thrombocytopenia in patients with severe acute respiratory syndrome (review). Hematology **2005**; 10:101–5.

30. Tang N, Bai H, Chen X, Gong J, Li D, Sun Z. Anticoagulant treatment is associated with decreased mortality in severe coronavirus disease 2019 patients with coagulopathy. J Thromb Haemost **2020**; 18:1094–9.

31. Li H, Liu L, Zhang D, et al. SARS-CoV-2 and viral sepsis: observations and hypotheses. Lancet **2020**; 395:1517–20.

32. Solomon IH, Normandin E, Bhattacharyya S, et al. Neuropathological features of covid-19. N Engl J Med **2020**; 383:989–92.

33. Nepal G, Rehrig JH, Shrestha GS, et al. Neurological manifestations of COVID-19: a systematic review. Crit Care **2020**; 24:421.

34. Guan WJ, Liang WH, Zhao Y, et al. Comorbidity and its impact on 1590 patients with COVID-19 in China: a nationwide analysis. Eur Respir J **2020**; 55:2000547.

35. Richardson S, Hirsch JS, Narasimhan M, et al. Presenting characteristics, comorbidities, and outcomes among 5700 patients hospitalized with COVID-19 in the New York City area. JAMA **2020**; 323:2052–9.